This is the Pre-Published Version.

Y. Chen, S. Lin, Z. Liang, X. Huang (2022) *Clean Smoldering Biowaste Process: Effect of Burning Direction on Smoke Purification by Self-Sustained Flame*, **Fuel Processing Technology**, 237, 107453. https://doi.org/10.1016/j.fuproc.2022.107453

Clean Smoldering Biowaste Process: Effect of Burning Direction on Smoke Purification by Self-Sustained Flame

Yuying Chen[a,c], Shaorun Lin[a,b,*], Zhirong Liang[a], Xinyan Huang[a,*]

[a] *Department of Building Environment and Energy Engineering, The Hong Kong Polytechnic University, Hong Kong*

[b] *The Hong Kong Polytechnic University Shenzhen Research Institute, Shenzhen, China*

[c] *School of Civil and Environmental Engineering, University of Technology Sydney, Sydney, Australia*

**Corresponding to xy.huang@polyu.edu.hk (XH); flynn.lin@connect.polyu.hk (SL)*

Abstract

Smoldering is an attractive biowaste removal technology, but its toxic pollutions are significant concerns. This work explores smoldering biowaste removal with the emissions purified by a self-sustained flame and the effect of smoldering direction. The smoldering direction and intensity are controlled by the ignition position and upward internal airflow velocity (5-24 mm/s). We found that the flame can be sustained above the smoldering fronts to purify the smoldering emissions in different burning directions, and the flame duration and burnt mass fraction are much larger for the opposed smoldering. To sustain a flame above an opposed smoldering front, the minimum airflow velocity is 6 mm/s, and the minimum smoldering burning flux is 10 ± 1 g/m^2·s. Comparatively, sustaining a flame above a forward smoldering requires a larger airflow velocity (~11 mm/s) and smoldering intensity (>16 g/m^2·s). Therefore, the flame is easier to remove more emissions from opposed smoldering which is recommended for the waste removal process. The critical smoldering burning flux at flame extinction is constant at 9 ± 1 g/m^2·s, regardless of the smoldering direction and airflow velocity. This work deepens the understanding of the co-existence of smoldering and flaming and enriches strategies for environmentally friendly smoldering waste removal technologies.

Keywords: Clean waste treatment; Smoldering emissions; Propagation mode; Woody waste.

Graphical abstract

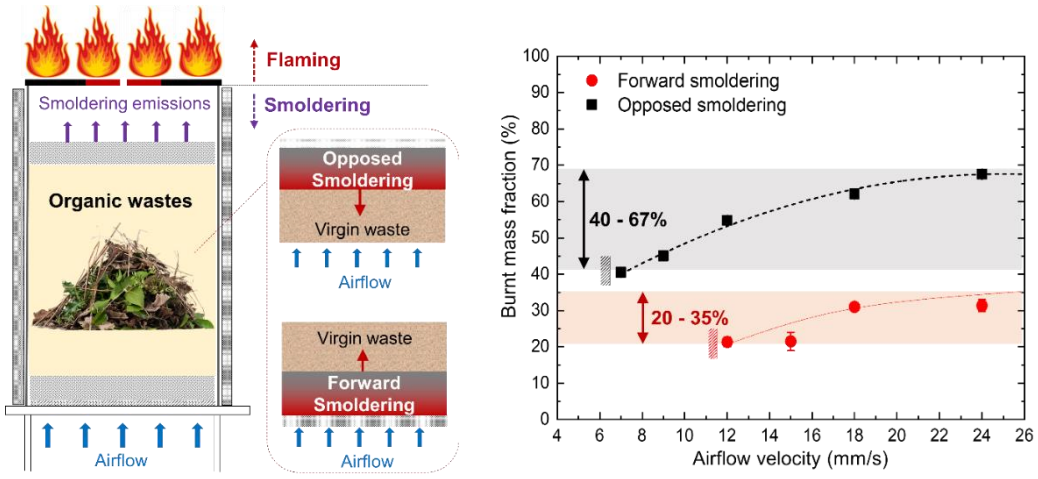

1. Introduction

Smoldering is low-temperature, flameless, and persistent burning of porous fuels, which is different from flaming in terms of transport processes and time scales [1–3]. Fundamentally, smoldering is a heterogeneous oxidative process sustained when oxygen molecules directly attack a hot charring surface, so it is the driving combustion phenomenon of reactive porous media like wood [4,5], coal [6], incense [7,8], cotton [9], and peat [10–13]. Once ignited, smoldering can sustain in extreme conditions such as poor oxygen supply and large fuel moisture content (MC). Generally, the characteristic temperature (500-800 ℃), propagation rate (~1 cm/h), and heat of combustion (~10 MJ/kg) of smoldering are lower than those of flaming [1,2].

In recent years, smoldering combustion has been adopted as one of the most applicable alternatives for traditional organic waste removal technologies (e.g., incineration [14,15]), exhibiting excellent application prospects [1,16,17]. Currently, such a technique has been successfully applied to remove organic wastes with high moisture contents like bioliquid [18,19], feces [20,21], agricultural wastes [22], wastewater sludges [23], food wastes [24], and oil shales [25], as reviewed in [1]. Compared with the traditional methods, the smoldering-based waste removal method has been proved to have many advantages. Firstly, the combustion temperature of the smoldering reactor is relatively low, improving the safety of operation and removal process. Secondly, only minimum pre-treatment processes (e.g., drying and grinding) are required [20,26], lowering the cost of treatment. Thirdly, this technology has a great potential for improving process efficiency by controlling the oxygen supply [27].

On the other hand, as smoldering combustion is an incomplete burning phenomenon, many harmful emissions will be released during the process of biowaste treatment [5,10,28,29], and public concerns about environmental pollution and potential health risks have limited its further application and promotion. Emissions released from smoldering comprise carbon dioxide (CO_2), carbon monoxide (CO), methane (CH_4), hydrogen cyanide (HCN), volatile organic compounds (VOCs) and particulate matter (PM) [15,29–32]. Specifically, emission factors (EFs) of incomplete combustion products, like CO, CH_4, and VOCs are higher than flaming combustion [11]. Among all the smoldering emissions, a high level of CO is the most toxic and lethal, CO_2 and CH_4 are the most significant greenhouse gases, while NO_x and VOCs are the major precursors of O_3 and secondary organic aerosol after complex photochemical processes [33]. Therefore, it is of vital importance for us to explore new methods to mitigate the pollution from the smoldering-based removal technology and promote its application.

A typical smoldering front includes both pyrolysis and char-oxidation reactions, so it generates substantial flammable unburnt hydrocarbons and CO [11]. With a rich oxygen supply, these flammable emissions will be ignited, contributing to a smoldering-to-flaming (StF) transition process [34]. Moreover, smoldering can also co-exist with the flame [4,35], so there is a great potential for using a self-sustained flame without additional fuels and heat to remove these flammable and toxic smoldering emissions. In our previous work, we successfully verified the applicability of using a self-sustained flame to clean the emissions from the smoldering wood wastes, coffee wastes, and organic soil

(simulated sludge) under upward airflows (see Fig. 1) [5,10]. The purification effect of flame has been demonstrated, where the post-flaming emission has significantly lower CO and VOCs than the original smoldering emissions.

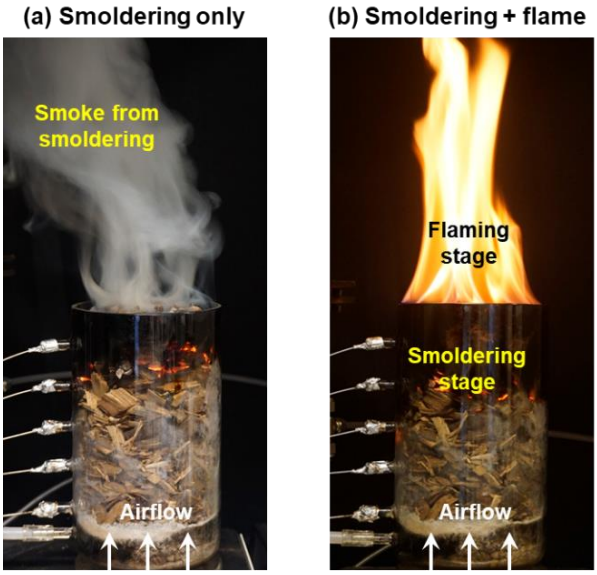

Fig. 1. Smoldering biowaste removal (a) without and (b) with a self-sustained flame to purify the smoke.

Fundamentally, smoldering combustion is controlled by the competition between oxygen supply and heat transfer to and from the reaction zone [35]. Depending on the relative direction between the propagation of the smoldering front and the oxidizer flow, smoldering processes are classified into two categories: forward and opposed smoldering [2]. Generally, the opposed spread is much faster than the forward spread, but its temperature is lower [36]. So far, most of the smoldering waste processes adopt the forward smoldering mode [10,23,37], while the opposed smoldering mode is rarely explored or compared. Therefore, whether different smoldering directions will affect the critical conditions of sustaining a flame above the smoldering front and the efficiencies of smoke purification are still poorly understood.

To fill this knowledge gap, this study aims to explore the impacts of smoldering directions on the critical conditions for maintaining a flame to purify the smoldering emissions. The experiments were conducted with wood wastes under various upward airflow velocities (5-24 mm/s) and two smoldering propagation directions (forward and opposed). The combustion phenomena, smoldering temperature and spread rate, smoldering burning flux, burnt mass fraction, and flaming ignition thresholds of different smoldering spread modes are quantified and analyzed.

2. Methods

2.1 Wood waste sample

Wood (or yard) waste is a common biowaste all over the world. For example, in Hong Kong, about 40,000 t of yard wastes (mostly tree wastes resulted from typhoons) are produced and directly sent to landfills annually, bringing great pressure to the limited land resources [38]. Thus, wood-chip waste

was chosen in this experiment, the same as our previous work (Fig. 2) [5]. The wood chips were provided by a local supplier (ECO-Greentech Ltd.), and their particle sizes range from 20 mm to 30 mm with an average of 25 mm. The dry bulk density, solid density, and porosity were measured to be 210 ± 10 kg/m^3, 600 ± 20 kg/m^3, and 0.65, respectively. The element analysis of the wood sample shows 36.6, 3.73, 59.47, 0.44, and 0.06 % mass fractions for C, H, O, N and S, respectively. Before the test, the raw wood chips were thoroughly dried in an oven at 90 °C for 48 h, and their moisture contents were measured to be <8% when reaching a new equilibrium with ambient moisture. The thermal analysis for the wood samples was conducted with a PerkinElmer STA 6000 Simultaneous Thermal Analyzer in both air and N_2 atmospheres, and the representative data are shown in Fig. A1.

2.2 Experimental setup

Fig. 2(a) shows the schematic diagram of the experimental setup, which included a cylindrical smoldering reactor, an electrical balance, an ignition system, and an air supply system. The open-top reactor was made of 3-mm thick aluminum alloys, and it had a depth of 20 cm and an internal diameter of 14 cm. A 1-cm thick ceramic insulation layer was attached to the outer surface of the reactor to reduce the lateral heat losses.

At the bottom of the burner, there is a 5-cm deep air mixer to straighten and homogenize the upward airflow. The burning area of the reactor and the air mixer are separated by a steel mesh and a 4-cm gravel layer. Before the experiment, a wood waste sample with a controlled mass of 420 ± 10 g was placed on the gravel layer with a constant height of 15 cm. To monitor the temperature and trace the position of the smoldering front, an array of eight K-type thermocouples (1.5 mm bead diameter) was inserted into the fuel along the axis from 0 cm (bottom) to 14 cm (top) with an interval of 2 cm. A top-view GoPro camera was used to record the test.

2.3 Experimental procedure

Initially, 70-g pre-ignited wood chips were used to initiate smoldering for all experiments at a constant upward airflow velocity of 10 mm/s. The ignition was applied at the top surface of the wood chips to initiate an opposed smoldering, while the ignition was applied at the bottom surface of the fuel bed to initiate a forward smoldering (see Fig. 2b). After successful ignition (a uniform and thin layer of smoke occurred on the top of the burner), a layer of fine and clean gravel with a height of 3 cm was placed on the top fuel surface. Then, the supply rate of upward forced airflow was adjusted by controlling the flow meter. For both ignition positions, the experiments were performed at various upward airflow velocities (u) ranging from 5 mm/s to 24 mm/s. Note that the airflow velocity was an overall value of the cross-section, and considering the porosity of 0.65, the average velocity through the pores was from 7.7 mm/s to 37 mm/s.

Afterward, a lighter or a spark was applied near the top outlet of the reactor, aiming to ignite the emissions emitted from smoldering. The test was initially started with the largest airflow velocity. If the smoldering emissions were successfully ignited and the flame became self-sustained, the flow

velocity was gradually decreased to find the limiting conditions. The experiments were stopped when all thermocouples were below 100 °C. For each scenario, at least two repeating tests were conducted, and for the tests near the limits, three or four repeating tests were conducted to ensure repeatability. During the experiments, the ambient temperature was 22±2 °C, the relative humidity was 50±10%, and the ambient pressure was 101 kPa.

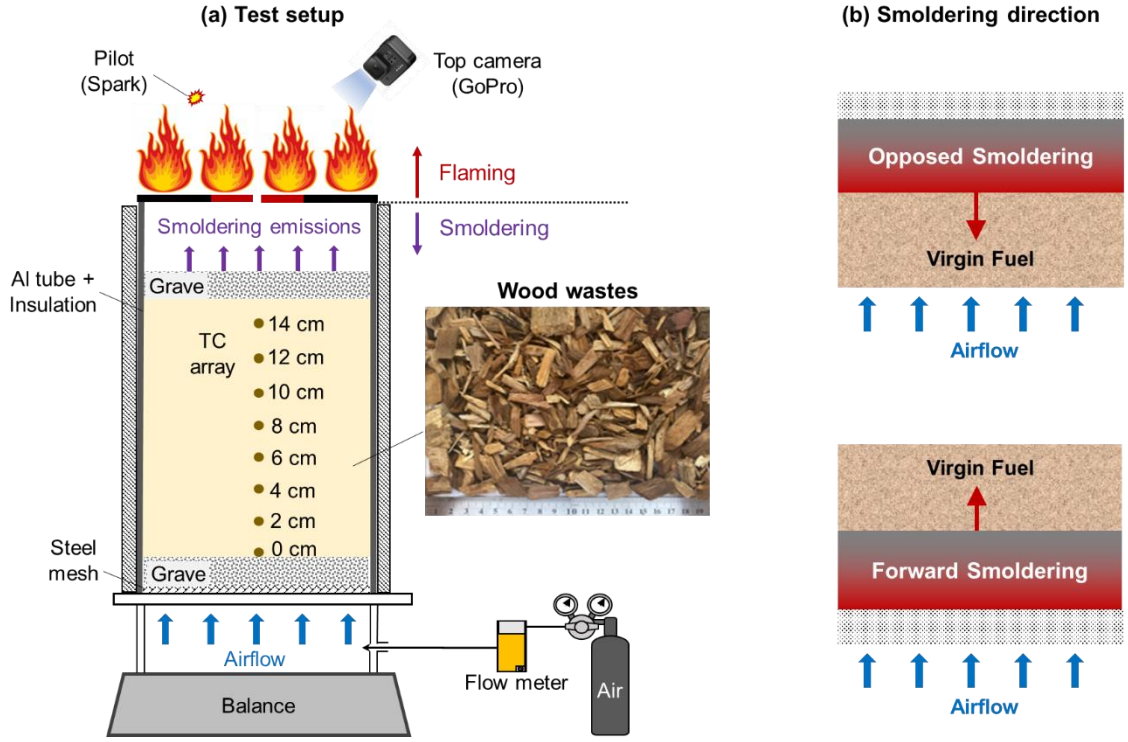

Fig. 2. Schematic diagrams of (a) the test setup, and (b) smoldering direction.

3. Results and discussion

3.1 Combustion phenomena

Fig. 3 compares the combustion phenomena of the forward and opposed smoldering at a consistent internal upward airflow velocity of 24 mm/s (see Videos S1 and S2). In both smoldering modes, a flame could be piloted and sustained at the outlet of the burner, co-existing with the smoldering combustion underneath. Therefore, we successfully demonstrated that a stable flame could be sustained above the opposed and forward smoldering fronts to remove emissions from smoldering wood wastes.

For the forward smoldering (Fig. 3a), there was a short and unstable flash flame that lasted for a very short period (about 20 s) when a spark was applied, because of the continuous pyrolysis of the 70-g pre-ignited fuels. Such a flash was an ignition effect and was not considered as a self-sustained flame. During this transition stage (< 8 min), the smoke plume was heavy but was not flammable enough because of the insufficient flammable components and large amounts of CO_2, H_2O, and large-molecule VOCs in the smoke. Later, even if the flame became continuous, some unburnt smoke still leaked out

from the flame. In contrast, for the opposed smoldering (Fig. 3b), once piloted, the flame above the opposed smoldering front became stable with almost all visible smoke removed, similar to the observations in our previous works [5,10].

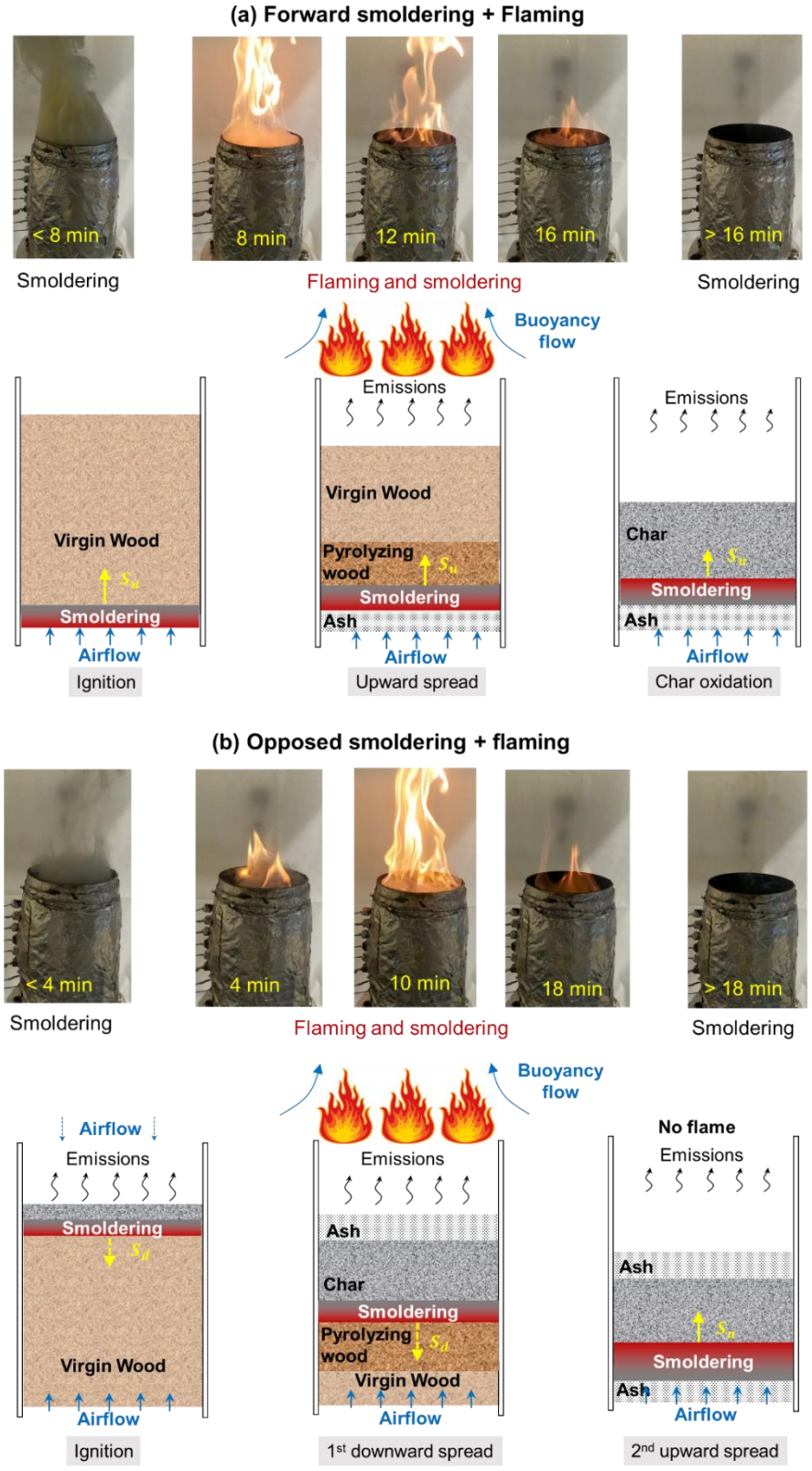

Fig. 3. Flaming phenomena and diagrams of (a) forward smoldering and (b) opposed smoldering under the upward airflow of 24 mm/s (see more details in Videos S1 and S2).

More importantly, the self-sustained flame ignited on the emissions from opposed smoldering appeared earlier and burned more stably and intensively. Fig. 4 further summarizes the flaming durations for both smoldering directions under different airflow velocities, where the flame duration above opposed smoldering is longer than that of forward smoldering and shows inverse trends with airflow velocity.

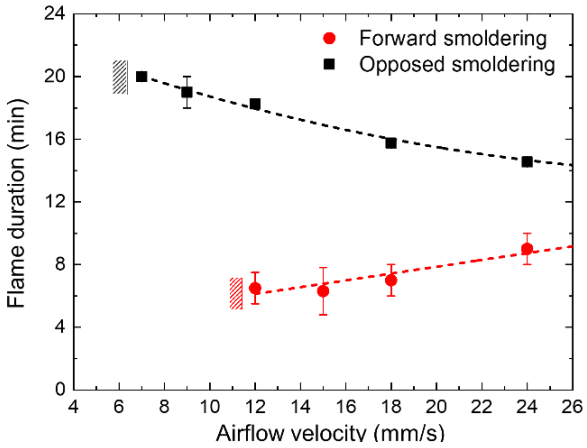

Fig. 4 The flaming duration above forward and opposed smoldering vs. airflow velocity.

Such different flame phenomena above the smoldering fronts were related to the smoldering propagation processes and reaction sub-fronts. A complete smoldering front includes a drying sub-front, a fuel pyrolysis sub-front, and a char oxidation sub-front, among which the pyrolysis sub-front produces the most flammable emissions that contribute to sustaining a flame. For the forward smoldering, the pyrolysis is driven by an intense char-oxidation sub-front that has a higher temperature (>700 °C in Fig. 5a), and the pyrolysis front moves together with the smoldering front without fast expansion to generate more pyrolysis gases (a single-stage smoldering process). Such smoldering propagation phenomenon has also been observed in previous experiments [13,39]. Thus, the pyrolysis co-exists with an extensive char oxidation process where a large number of incombustible gases (e.g., H_2O and CO_2) may lower the flammability of the emissions.

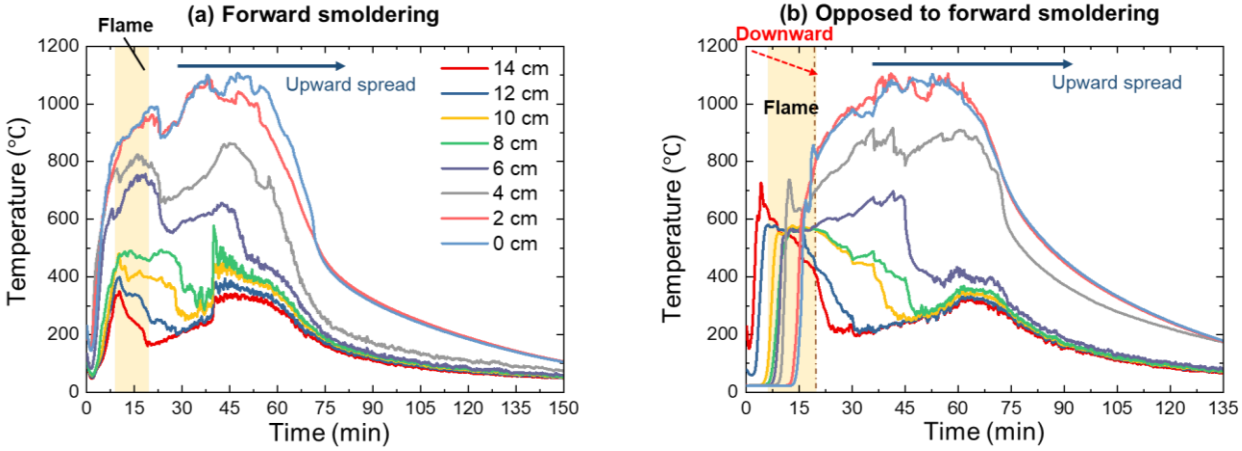

Fig. 5. Smoldering temperature profiles of (a) forward smoldering and (b) opposed smoldering and the transition to 2nd-forward smoldering under the airflow velocity of 18 mm/s.

For the opposed smoldering, the pyrolysis sub-front is driven by a low-temperature oxidation sub-front towards the direction of oxygen supply (<600 °C up to 16 min in Fig. 5b). During this process, the pyrolysis front expanded and spread downwards rapidly, which has been demonstrated in previous experiments [36,39], leaving behind a thick char layer (1st-stage opposed smoldering process). Such a process is a continuous smoldering ignition process that is controlled by heat transfer [35,40]. Therefore, the smoke from opposed smoldering primarily contains pyrolyzates from wood pyrolysis (e.g., CH_4, C_2H_4, C_2H_6, and CO), which are highly flammable, making it much easier to be ignited than that from forward smoldering. Afterward, most of the char produced from pyrolysis remains that are further oxidized in the 2nd-stage upward smoldering with a higher temperature, while this process cannot sustain a flame above. Another possible reason for the difference in the flame above is that the hot opposed smoldering front is near the top surface of the fuel bed which can better support the flame above, whereas the top of the fuel bed will be cooler as the forward smoldering front is further below the surface.

3.2 Smoldering temperature and spread rate

Fig. 6a shows the peak temperatures of the single-stage forward smoldering and the two-stage opposed-to-forward smoldering under varying airflow velocities. Fig. 6b shows the average smoldering burning rates (both spread rate of the pyrolysis front and burning speed) estimated from the temperature profiles. Specifically, the average spread rate of the pyrolysis front is estimated by tracking the moments when TC (0 cm) and TC (14 cm) reach 300 °C, which is shown as the hollow symbols in Fig. 6b. And burning speed is defined as the surface regression speed of the fuel bed, which is estimated by dividing the fuel height by the time when the bottom TC (0 cm) starts to decrease, which is shown as the solid symbols in Fig. 6b. As expected, both the peak temperatures and the smoldering spread rates increase with the airflow velocity because of stronger char oxidation under a better oxygen supply.

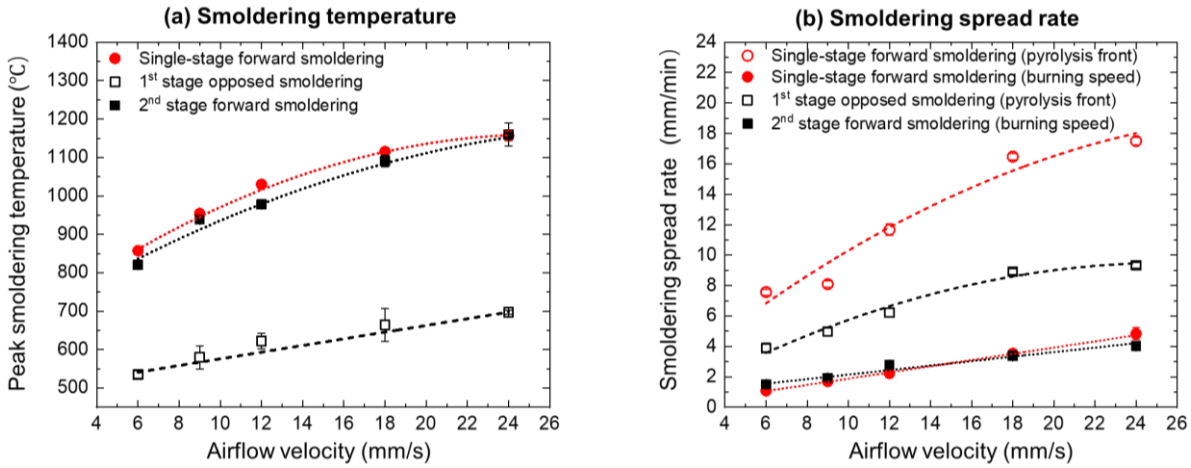

Fig. 6. (a) Peak smoldering temperatures and (b) average smoldering spread rates of forward smoldering and the opposed-to-forward smoldering vs. airflow velocities.

Moreover, Fig. 6a shows the peak temperature of the single-stage forward smoldering is slightly larger than that of the 2nd-stage forward smoldering, and both are significantly larger than the 1st-stage opposed smoldering. This is because the 1st-stage opposed smoldering is a fast-expanding process of pyrolysis front where the char oxidation is weak, resulting in a lower peak temperature [36,39]. Fig. 6b shows that the spread rate of the single-stage forward pyrolysis front is larger than that of the 1st-stage opposed pyrolysis front, while the average burning speeds for both single-stage forward smoldering and 2nd stage forward smoldering are similar. Noted that the burning speed may be slightly overestimated as the fuel bed at this moment may slightly regress, but the overall trend is not affected.

3.3 Smoldering burning flux

The burning flux ($\dot{m}''$) is the mass loss rate per unit area of the fuel, which is an important parameter to quantify the combustion limits. Fig. 7a-b compares the time evolution of the remaining mass fraction and the burning flux of wood under the forward smoldering and opposed smoldering under the airflow velocity of 18 mm/s. The profiles of the burning flux for both spread modes are similar: during the initial stage, the burning flux increases rapidly, reaching a peak value in a short time. Afterward, it dramatically decreases and remains at a low value of about 2-4 g/m^2·s for a longer period until burnout occurs.

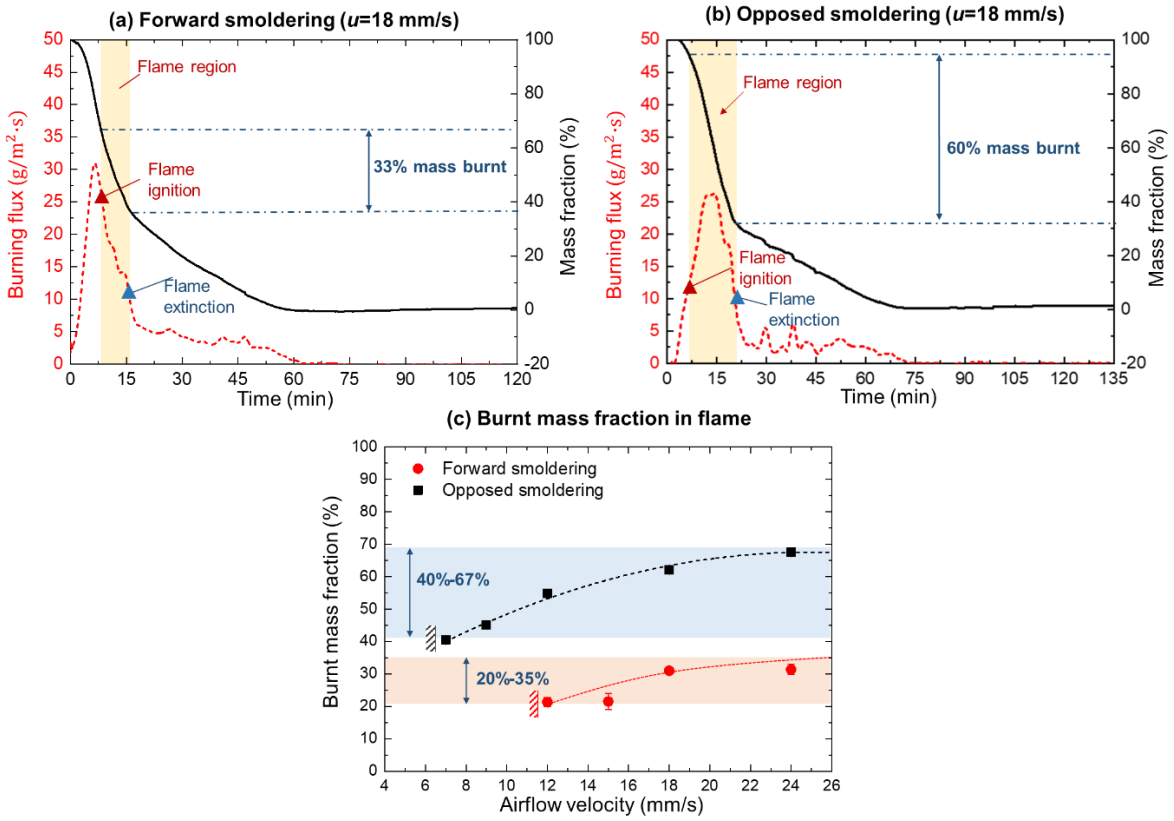

Fig. 7. Evolution of smoldering burning flux of (a) forward smoldering and (b) opposed smoldering at the airflow velocity of 18 mm/s, and (c) the burnt mass fraction during the co-existence of flame in different smoldering propagation modes under various airflow velocities.

The red triangle symbols in Fig. 7a-b represent the critical smoldering burning flux for flame ignition ($\dot{m}''_{ig}$), which is determined as the value of the burning flux at the moment when a self-sustained flame is piloted on the smoldering emissions, and the blue triangle symbols signify the critical burning flux for flame extinction (or the self-sustained flame disappears) ($\dot{m}''_{ex}$). For forward smoldering (Fig. 7a), the flame ignition occurs during the decrease period of the smoldering burning flux, at which the critical burning flux reaches about 27 g/m^2·s, and then disappears as the burning flux decreases to about 10 g/m^2·s.

However, for the opposed smoldering (Fig. 7b), the flame is ignited when the burning flux rises to about 11 g/m^2·s, and then extinguishes as the burning flux decreases to about 9 g/m^2·s. During the flame period, 60 % mass of the wood is burnt by opposed smoldering, while only 33 % mass fraction is burnt by the forward smoldering. Fig. 7c further summarizes the burnt mass fraction in the flaming period under various airflow velocities. Clearly, the burnt mass fraction in both modes of smoldering propagation increases as the airflow velocity increases. More importantly, it is observed that the burnt mass fraction in the period of co-existed flame above opposed smoldering (40 %-67 %) is significantly larger than that above forward smoldering (20 %-35 %), indicating the opposed smoldering is more efficient for our proposed waste removal method.

3.4 Flaming limits for smoldering emissions

Fig. 8 summarizes the critical smoldering burning flux for flame ignition ($\dot{m}''_{ig}$) and flame extinction ($\dot{m}''_{ex}$), as well as the maximum smoldering flux ($\dot{m}''_{max}$) under various airflow velocities of different spread modes. Firstly, it is observed in Fig. 8a that a larger airflow velocity (~11 mm/s) is required for the emissions from forward smoldering to be ignited as a stable flame compared with that of opposed smoldering (~6 mm/s). Secondly, Fig. 8a shows the critical burning flux for flame ignition above the opposed smoldering front is almost constant at about 10 g/m^2·s, while the critical burning flux for flame ignition above the forward smoldering shows an increasing trend with the airflow velocity (increases from 16 g/m^2·s to 29 g/m^2·s as the airflow velocity increases from to 12 mm/s to 24 mm/s). Thirdly, the critical burning flux for flame extinction (Fig. 8b) in both smoldering modes is similar at about 9±1 g/m^2·s (hollow markers), which is slightly lower than that for flame ignition above opposed smoldering (solid markers). It should be emphasized that the critical airflows required to reach such critical smoldering burning fluxes may vary at different experimental scales.

Moreover, Fig. 8c shows that the maximum burning flux of forward smoldering is slightly larger than opposed smoldering, and both of them increase as the airflow velocity increases. Although the opposed smoldering burns wood wastes slightly slower, the emissions are much easier to be cleaned by a co-existed flame above it. Moreover, the flame duration above opposed smoldering is longer, which covers a larger burning fraction of wood, and the required airflow velocity for opposed smoldering is smaller.

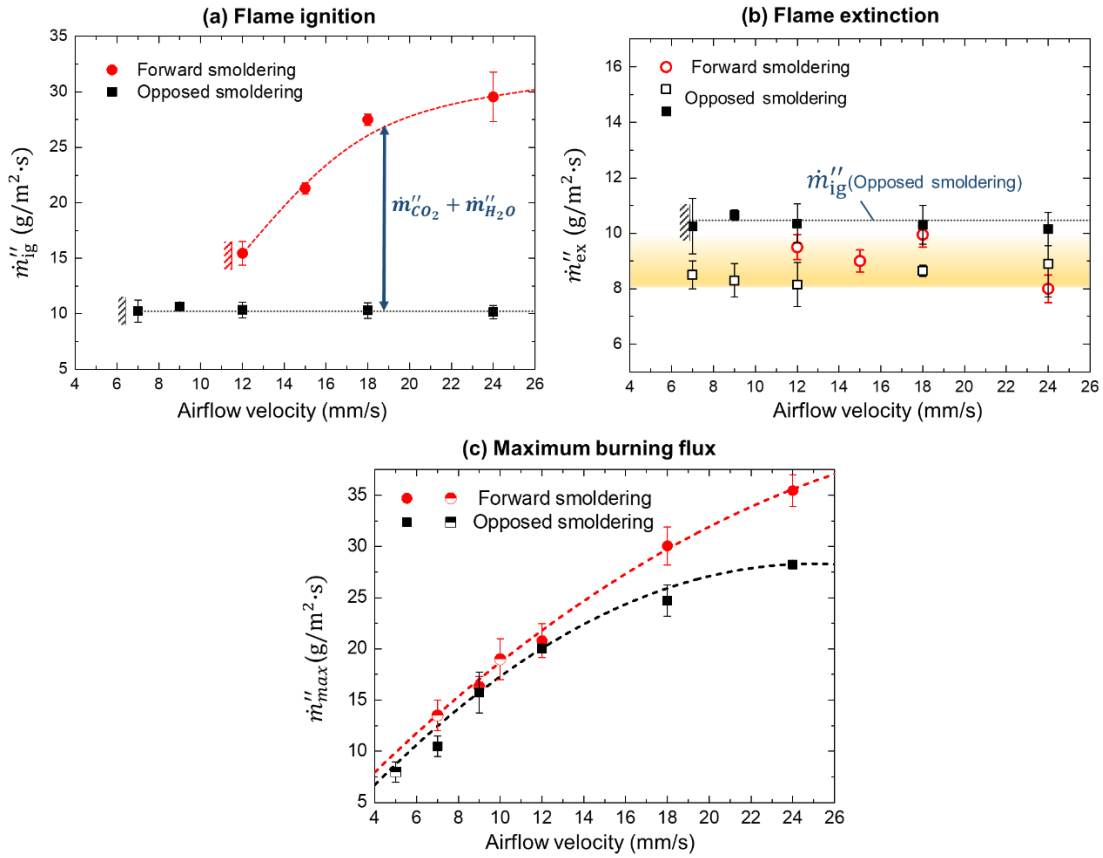

Fig. 8. Critical smoldering burning flux for (a) flame ignition, (b) flame extinction, where flammability limits above opposed smoldering front (solid markers) are presented for comparison, and (c) maximum smoldering burning flux, where the solid makers represent flaming cases, and hemi-solid markers represent no-flame cases.

To ignite and maintain a flame, a minimum mass flux of fuel gas is required. In this experiment, the fuel gas to sustain a flame in smoldering emissions is mainly the hydrocarbons and CO released from the wood pyrolysis. Here, a simplified heat transfer analysis is introduced for the flame above the smoldering front. The flame heat release rate ($\dot{q}''_f$) by burning the pyrolysis gases should at least overcome the heat loss to the environment ($\dot{q}''_\infty$) and burner wall ($\dot{q}''_w$) as

$$\dot{q}''_f = \dot{m}''_{py,crt}\Delta H_f = \dot{q}''_\infty + \dot{q}''_w \quad (1)$$

where $\dot{m}''_{py,crt}$ is the minimum mass flux of pyrolysis gases, and ΔH_f is the heat of flaming combustion.

For the opposed smoldering, the dominant reaction within the smoldering front is the wood pyrolysis, which has been studied and proven in previous studies [36,39]. In this way, the small amount of emissions from char oxidation (e.g. CO_2 and H_2O) can be ignored and the total smoldering emissions ($\dot{m}''_{sm}$) can be approximately regarded as all pyrolysis gas [10], that is, $\dot{m}''_{py} \approx \dot{m}''_{sm}$. Therefore, the required critical smoldering burning flux for a flame to be ignited above the opposed smoldering is a constant value as

$$\dot{m}''_{ig,opp} = \dot{m}''_{sm,crt} = \dot{m}''_{py,crt} = \frac{\dot{q}''_\infty + \dot{q}''_w}{\Delta H_f} \quad (2)$$

In this paper, this constant value is found to be about 11 g/m^2·s, as shown in Fig. 8a.

However, for the forward smoldering, because the pyrolysis sub-front only moves with the char-oxidation sub-front gradually, apart from wood pyrolysis, char oxidation also plays an important role within the smoldering front [35,41]. Thus, the non-flammable H_2O and CO_2 released from oxidation cannot be ignored, which may inhibit the flame. At this moment, the total smoldering emissions ($\dot{m}''_{sm}$) include significant amounts of H_2O and CO_2 ($\dot{m}''_{sm} = \dot{m}''_{py} + \dot{m}''_{CO_2} + \dot{m}''_{H_2O}$). Then, Eq. (1) is re-arranged as

$$(\dot{m}''_{sm,crt} - \dot{m}''_{CO_2} - \dot{m}''_{H_2O})\Delta H_f = \dot{q}''_{\infty} + \dot{q}''_{w} \tag{3}$$

Therefore, the critical smoldering burning flux for a flame to be ignited above the forward smoldering is expressed as

$$\dot{m}''_{ig,for} = \dot{m}''_{sm,crt} = \frac{\dot{q}''_{\infty} + \dot{q}''_{w}}{\Delta H_f} + \dot{m}''_{CO_2} + \dot{m}''_{H_2O} \tag{4}$$

Eq. (4) and Eq. (2) explain why the critical burning flux in for flame ignition above the forward smoldering ($\dot{m}''_{ig,for}$) is larger than the opposed smoldering ($\dot{m}''_{ig,opp}$). Moreover, as the oxidation intensity increases with the airflow velocity, which results in an increase in $\dot{m}''_{CO_2}$ and $\dot{m}''_{H_2O}$. This also explains why $\dot{m}''_{ig,for}$ shows a significant increase with airflow velocity in Fig. 8a. In our future work, the comparison of smoldering emissions from forward and opposed smoldering will be comprehensively compared, and tests at different scales will be conducted to demonstrate the scalability.

4. Conclusions

In this work, we successfully applied a self-sustained flame above both the forward and opposed smoldering fronts to purify the toxic smoldering emissions. It is found that the emission gases from opposed smoldering are much easier to be ignited, and the flame duration and burnt mass fraction are much larger than that of the forward smoldering. The flame sustained above the smoldering is influenced by the competition reactions between wood pyrolysis and char oxidation within the smoldering front. For opposed smoldering, due to a fast-expanding pyrolysis zone, significant amounts of flammable pyrolyzates are released, making its emissions highly flammable. However, the forward smoldering front includes both slow wood pyrolysis and intense char oxidation, making the emissions less flammable because of fewer pyrolyzates and excessive CO_2 and H_2O from char oxidation.

To sustain a stable flame above opposed smoldering, the minimum airflow velocity required is about 6 mm/s, and the minimum smoldering burning flux is 10 ± 1 g/m^2·s. Comparatively, sustaining a flame above forward smoldering front requires a larger airflow velocity (~11 mm/s), and the minimum smoldering burning flux is not constant but increases with the airflow velocity. Moreover, the critical smoldering burning flux at flame extinction is constant at 9 ± 1 g/m^2·s, regardless of the smoldering direction and airflow velocity. A theoretical analysis based on the simplified heat transfer process

successfully explains the trends between the critical burning flux for flame ignition and the smoldering propagation modes.

This work deepens the understanding of the co-existence of smoldering and flaming, enriches the theory for the clean treatment of smoldering emissions via its re-combustion, and promotes an energy-efficient and environmentally friendly method for biowaste removal. Future works will quantify and compare the emission gases and the efficiency of smoke purification in different smoldering propagation modes and conduct experiments at different scales.

CRediT authorship contribution statement

Yuying Chen: Investigation, Writing-original draft, Formal analysis.

Shaorun Lin: Investigation, Resources, Formal analysis, Writing-review & editing.

Zhirong Liang: Investigation, Supervision, Resources.

Xinyan Huang: Conceptualization, Supervision, Writing-review & editing, Funding acquisition.

Declaration of Competing Interest

The authors declare that there is no conflict of interest.

Acknowledgements

This work is funded by National Natural Science Foundation of China (NSFC grant No. 51876183), ZJU SKLCEU Open Fund (2018012), and Sichuan Science and Technology Program (2019YFSY0040). Authors thanks ECO-Greentech Ltd. for providing fuel samples.

References

[1] J.L. Torero, J.I. Gerhard, M.F. Martins, M.A.B. Zanoni, T.L. Rashwan, J.K. Brown, Processes defining smouldering combustion: Integrated review and synthesis, Progress in Energy and Combustion Science. 81 (2020) 100869. https://doi.org/10.1016/j.pecs.2020.100869.

[2] G. Rein, Smoldering Combustion, SFPE Handbook of Fire Protection Engineering. 2014 (2014) 581–603. https://doi.org/10.1007/978-1-4939-2565-0_19.

[3] T.J.T.J. Ohlemiller, Modeling of smoldering combustion propagation, Progress in Energy and Combustion Science. 11 (1985) 277–310. https://doi.org/10.1016/0360-1285(85)90004-8.

[4] S. Lin, X. Huang, J. Gao, J. Ji, Extinction of Wood Fire: A Near-Limit Blue Flame Above Hot Smoldering Surface, Fire Technology. 58 (2022) 415–434. https://doi.org/10.1007/s10694-021-01146-6.

[5] Y. Chen, Z. Liang, S. Lin, X. Huang, Limits of sustaining a flame above smoldering woody biomass, Combustion Science and Technology. (2022). https://doi.org/10.1080/00102202.2022.2041000.

[6] D. Wu, X. Huang, F. Norman, F. Verplaetsen, J. Berghmans, E. Van Den Bulck, Experimental investigation on the self-ignition behaviour of coal dust accumulations in oxy-fuel combustion system, Fuel. 160 (2015) 245–254. https://doi.org/10.1016/j.fuel.2015.07.050.

[7] S. Lin, T.H. Chow, X. Huang, Smoldering propagation and blow-off on consolidated fuel under external airflow, Combustion and Flame. 234 (2021) 111685. https://doi.org/10.1016/j.combustflame.2021.111685.

[8] T. Yamazaki, T. Matsuoka, Y. Li, Y. Nakamura, Applicability of a Low-Pressure Environment to Investigate Smoldering Behavior Under Microgravity, Fire Technology. (2020). https://doi.org/10.1007/s10694-019-00911-y.

[9] Q. Xie, Z. Zhang, S. Lin, Y. Qu, X. Huang, Smoldering Fire of High-Density Cotton Bale Under Concurrent Wind, Fire Technology. 56 (2020) 2241–2256. https://doi.org/10.1007/s10694-020-00975-1.

[10] Y. Chen, S. Lin, Z. Liang, N.C. Surawski, X. Huang, Smouldering Organic Waste Removal Technology with Smoke Emissions Cleaned by Self-Sustained Flame, Journal of Cleaner Production. 368 (2022). https://doi.org/10.1016/j.jclepro.2022.132363.

[11] Y. Hu, E. Christensen, F. Restuccia, G. Rein, Transient gas and particle emissions from smouldering combustion of peat, Proceedings of the Combustion Institute. 37 (2019) 4035–4042. https://doi.org/10.1016/j.proci.2018.06.008.

[12] X. Huang, G. Rein, Thermochemical conversion of biomass in smouldering combustion across scales: The roles of heterogeneous kinetics, oxygen and transport phenomena, Bioresource Technology. 207 (2016) 409–421. https://doi.org/10.1016/j.biortech.2016.01.027.

[13] X. Huang, G. Rein, Downward spread of smouldering peat fire: The role of moisture, density and oxygen supply, International Journal of Wildland Fire. 26 (2017) 907–918. https://doi.org/10.1071/WF16198.

[14] J. He, L. Li, H. Feng, M. Jiang, J. Li, L. Guo, J. Zhang, P. Zhang, J. Gong, Q. Huang, Morphology and nanostructure of flame-formed soot particles from combustion of typical municipal solid waste, Fuel Processing Technology. 232 (2022) 107269. https://doi.org/10.1016/j.fuproc.2022.107269.

[15] Z. Zhou, X. Qiu, Y. Wang, Y. Duan, L. Li, H. Lin, Y. Luo, Z. Sun, L. Duan, Particulate matter formation during shoe manufacturing waste combustion in a full-scale CFB boiler, Fuel Processing Technology. 221 (2021) 106914. https://doi.org/10.1016/j.fuproc.2021.106914.

[16] B.J. WYN H K, KONAROVA M, H.K. Wyn, M. Konarova, J. Beltramini, G. Perkins, L. Yermán, Self-sustaining smouldering combustion of waste: A review on applications, key parameters and potential resource recovery, Fuel Processing Technology. 205 (2020) 106425. https://doi.org/10.1016/j.fuproc.2020.106425.

[17] T.L. Rashwan, T. Fournie, L. Torero, G.P. Grant, J.I. Gerhard, Scaling up self-sustained smouldering of sewage sludge for waste-to-energy Distance, 135 (2021) 298–308. https://doi.org/10.1016/j.wasman.2021.09.004.

[18] M.A.B. Zanoni, J.L. Torero, J.I. Gerhard, The role of local thermal non-equilibrium in modelling smouldering combustion of organic liquids, Proceedings of the Combustion Institute. 37 (2019) 3109–3117. https://doi.org/10.1016/j.proci.2018.05.177.

[19] L. Kinsman, J.L. Torero, J.I. Gerhard, Organic liquid mobility induced by smoldering remediation, Journal of Hazardous Materials. 325 (2017) 101–112. https://doi.org/10.1016/j.jhazmat.2016.11.049.

[20] L. Yermán, R.M. Hadden, J. Carrascal, I. Fabris, D. Cormier, J.L. Torero, J.I. Gerhard, M. Krajcovic, P. Pironi, Y.-L. Cheng, Smouldering combustion as a treatment technology for faeces : exploring the parameter space, Fuel. 147 (2015) 108–116. https://doi.org/10.1016/j.fuel.2015.01.055.

[21] I. Fabris, D. Cormier, J.I. Gerhard, T. Bartczak, M. Kortschot, J.L. Torero, Y.-L. Cheng, Continuous, self-sustaining smouldering destruction of simulated faeces, Fuel. 190 (2017) 58–66. https://doi.org/10.1016/j.fuel.2016.11.014.

[22] X. Cheng, Z. Huang, Z. Wang, C. Ma, S. Chen, A novel on-site wheat straw pretreatment method: Enclosed torrefaction, Bioresource Technology. 281 (2019) 48–55. https://doi.org/10.1016/j.biortech.2019.02.075.

[23] C. Feng, J. Huang, C. Yang, C. Li, X. Luo, X. Gao, Y. Qiao, Smouldering combustion of sewage sludge: Volumetric scale-up, product characterization, and economic analysis, Fuel. 305 (2021) 121485. https://doi.org/10.1016/j.fuel.2021.121485.

[24] Z. Song, T. He, M. Li, D. Wu, F. You, Self-sustaining smoldering as a novel disposal approach for food waste with high moisture content, Fuel Processing Technology. 228 (2022) 107144. https://doi.org/10.1016/j.fuproc.2021.107144.

[25] M.F. Martins, S. Salvador, J.-F. Thovert, G. Debenest, Co-current combustion of oil shale–Part 1: Characterization of the solid and gaseous products, Fuel. 89 (2010) 144–151.

[26] T.L. Rashwan, J.I. Gerhard, G.P. Grant, Application of self-sustaining smouldering combustion for the destruction of wastewater biosolids, Waste Management. 50 (2016) 201–

212. https://doi.org/10.1016/j.wasman.2016.01.037.
[27] L. Yermán, H. Wall, J. Torero, J.I. Gerhard, Y.L. Cheng, Smoldering Combustion as a Treatment Technology for Feces: Sensitivity to Key Parameters, Combustion Science and Technology. 188 (2016) 968–981. https://doi.org/10.1080/00102202.2015.1136299.
[28] Y. Hu, N. Fernandez-Anez, T.E.L.L. Smith, G. Rein, Review of emissions from smouldering peat fires and their contribution to regional haze episodes, International Journal of Wildland Fire. 27 (2018) 293–312. https://doi.org/10.1071/WF17084.
[29] S.S. Amaral, J.A. de Carvalho Junior, M.A.M. Costa, T.G.S. Neto, R. Dellani, L.H.S. Leite, Comparative study for hardwood and softwood forest biomass: Chemical characterization, combustion phases and gas and particulate matter emissions, Bioresource Technology. 164 (2014) 55–63. https://doi.org/https://doi.org/10.1016/j.biortech.2014.04.060.
[30] R.J. Yokelson, R. Susott, D.E. Ward, J. Reardon, D.W.T. Griffith, Emissions from smoldering combustion of biomass measured by open-path Fourier transform infrared spectroscopy, Journal of Geophysical Research. 102 (1997) 18865. https://doi.org/10.1029/97JD00852.
[31] J.P. Wagner, K.L. Soderman, R. Konzen, Particle size distributions and heavy metals emissions from guayule fireplace logs, Bioresource Technology. 35 (1991) 209–216.
[32] H.K. Wyn, G. Perkins, Fuel Gas Production From Self-Sustaining Smouldering Combustion of Lignocellulosic Waste, Research Square. (2021). https://doi.org/10.21203/rs.3.rs-817595/v1.
[33] S.P. Urbanski, W.M. Hao, S. Baker, Chapter 4 Chemical Composition of Wildland Fire Emissions, Developments in Environmental Science. 8 (2008) 79–107. https://doi.org/10.1016/S1474-8177(08)00004-1.
[34] M.A. Santoso, E.G. Christensen, J. Yang, G. Rein, Review of the Transition From Smouldering to Flaming Combustion in Wildfires, Frontiers in Mechanical Engineering. 5 (2019). https://doi.org/10.3389/fmech.2019.00049.
[35] X. Huang, J. Gao, A review of near-limit opposed fire spread, Fire Safety Journal. 120 (2021) 103141. https://doi.org/10.1016/j.firesaf.2020.103141.
[36] X. Huang, G. Rein, Upward-and-downward spread of smoldering peat fire, Proceedings of the Combustion Institute. 37 (2019) 4025–4033. https://doi.org/10.1016/j.proci.2018.05.125.
[37] L. Yermán, H. Wall, J.L. Torero, Experimental investigation on the destruction rates of organic waste with high moisture content by means of self-sustained smoldering combustion, Proceedings of the Combustion Institute. 36 (2017) 4419–4426. https://doi.org/10.1016/j.proci.2016.07.052.
[38] Y. Liu, S. Wu, H. Zhang, R. Xiao, Fast pyrolysis of holocellulose for the preparation of long-chain ether fuel precursors: Effect of holocellulose types, Bioresource Technology. 338 (2021) 125519. https://doi.org/10.1016/j.biortech.2021.125519.
[39] S. Lin, X. Huang, Quenching of smoldering: Effect of wall cooling on extinction, Proceedings of the Combustion Institute. 38 (2021) 5015–5022. https://doi.org/10.1016/j.proci.2020.05.017.
[40] T. Ohlemiller, D. Lucca, An experimental comparison of forward and reverse smolder propagation in permeable fuel beds, Combustion and Flame. 54 (1983) 131–147. https://doi.org/10.1016/0010-2180(83)90027-5.
[41] A.I. Bartlett, R.M. Hadden, L.A. Bisby, A Review of Factors Affecting the Burning Behaviour of Wood for Application to Tall Timber Construction, Fire Technology. 55 (2019) 1–49. https://doi.org/10.1007/s10694-018-0787-y.

Appendix

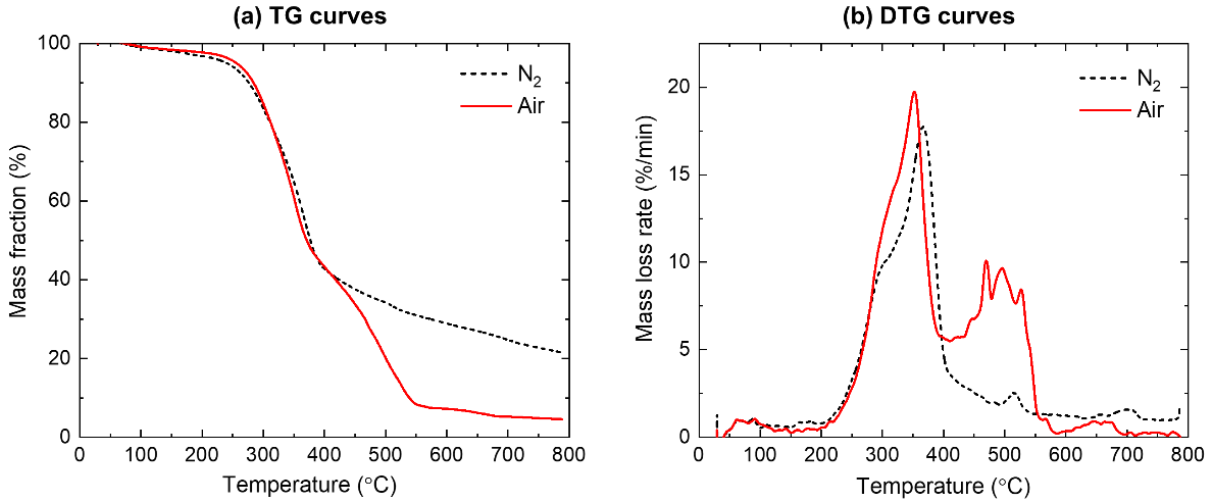

Fig. A1. TGA results of the wood chips at a heating rate of 30 K/min under air and nitrogen ambient.